Particles I

Access the latest eBook →

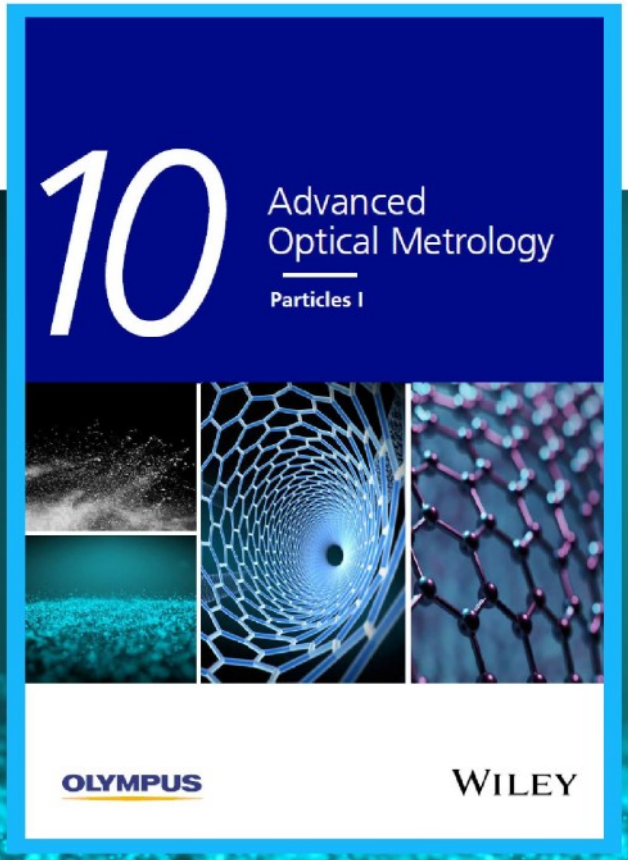

Particles: Unique Properties, Uncountable Applications

Read the latest eBook and better your knowledge with highlights from the recent studies on the design and characterization of micro- and nanoparticles for different application areas.

Access Now

This eBook is sponsored by

OLYMPUS

WILEY

ADVANCED FUNCTIONAL MATERIALS
www.afm-journal.de

Single Cell Bioprinting with Ultrashort Laser Pulses

Jun Zhang, Patrick Byers, Amelie Erben, Christine Frank, Levin Schulte-Spechtel, Michael Heymann, Denitsa Docheva, Heinz P. Huber, Stefanie Sudhop,* and Hauke Clausen-Schaumann**

Tissue engineering requires the precise positioning of mammalian cells and biomaterials on substrate surfaces or in preprocessed scaffolds. Although the development of 2D and 3D bioprinting technologies has made substantial progress in recent years, precise, cell-friendly, easy to use, and fast technologies for selecting and positioning mammalian cells with single cell precision are still in need. A new laser-based bioprinting approach is therefore presented, which allows the selection of individual cells from complex cell mixtures based on morphology or fluorescence and their transfer onto a 2D target substrate or a preprocessed 3D scaffold with single cell precision and high cell viability (93–99% cell survival, depending on cell type and substrate). In addition to precise cell positioning, this approach can also be used for the generation of 3D structures by transferring and depositing multiple hydrogel droplets. By further automating and combining this approach with other 3D printing technologies, such as two-photon stereolithography, it has a high potential of becoming a fast and versatile technology for the 2D and 3D bioprinting of mammalian cells with single cell resolution.

1. Introduction

The fabrication of 3D tissue substitutes will improve the treatment of lesions caused by injuries or diseases, as well as age related tissue degeneration.[1–4] Additionally, it has the potential of providing more relevant 3D test systems for drug development[1,4–6] and new insights into how cells interact with their environment and with one another.[3,7,8] In vivo, cells receive multiple biological, chemical, and physical stimuli from neighboring cells, the extracellular matrix (ECM), and the surrounding tissue. Cell behavior and fate crucially depend on these stimuli, many of which originate from their direct cell vicinity.[9–13] Controlling the cellular microenvironment in vitro with single cell precision is therefore an important factor for the generation of instructive cell environments and cell niches, which stimulate cells to migrate, differentiate, proliferate, and to form functional tissue.[14] In addition, the introduction of such detailed microenvironments will advance the fabrication of cell-chips and organs-on-a-chips and provide a better understanding of cell–cell interactions under normal and pathological conditions.[14–16] In recent years, numerous technologies have been developed to position mammalian cells in 2D and 3D.[17–20] However, the efficient and precise positioning of living cells at the single cell level still remains a major challenge. Currently, several inkjet-based and drop-on-demand approaches are investigated to place living cells on substrates with single cell precision.[21–23] However, these techniques suffer from limited accuracy and frequent cell damage. Acoustic cell patterning techniques like holographic cell patterning or standing surface acoustic waves provide high cell viability and achieve remarkable spatial resolution, while structuring large numbers of cells in a highly parallel approach.[24–28] Nevertheless, these techniques do not

J. Zhang, P. Byers, C. Frank, L. Schulte-Spechtel, Prof. H. P. Huber
Lasercenter
Munich University of Applied Sciences
Lothstrasse 34, 80335 Munich, Germany
E-mail: heinz.huber@hm.edu

J. Zhang, A. Erben, Dr. S. Sudhop, Prof. H. Clausen-Schaumann
Center for Applied Tissue Engineering and Regenerative Medicine
CANTER
Munich University of Applied Sciences
Lothstrasse 34, 80335 Munich, Germany
E-mail: stefanie.sudhop@hm.edu; hauke.clausen-schaumann@hm.edu

The ORCID identification number(s) for the author(s) of this article can be found under https://doi.org/10.1002/adfm.202100066.

DOI: 10.1002/adfm.202100066

J. Zhang, A. Erben, Prof. M. Heymann, Dr. S. Sudhop, Prof. H. Clausen-Schaumann
Center for NanoScience
University of Munich
80799 Munich, Germany

J. Zhang, Prof. D. Docheva
Experimental Trauma Surgery
Department of Trauma Surgery
University Regensburg Medical Centre
Am Biopark 9, 93053 Regensburg, Germany

A. Erben
Heinz-Nixdorf-Chair of Biomedical Electronics
TranslaTUM
Campus Klinikum rechts der Isar
Technical University of Munich
Einsteinstraße 25, 81675 Munich, Germany

Prof. M. Heymann
Institute of Biomaterials and Biomolecular Systems
University of Stuttgart
Pfaffenwaldring 57, 70569 Stuttgart, Germany

allow selectively targeting and manipulating individual cells, based on, for example, fluorescent markers, and positioning them arbitrarily with subcellular precision on a target surface or cell scaffold. Techniques, which allow for the reliable identification and selection of specific mammalian cells and the fast and accurate positioning of individual selected cells with high spatial resolution and cell viability, are still missing today.

We have therefore developed a method for the precise and efficient selection and positioning of individual mammalian cells, using ultrashort near infrared (NIR) laser pulses. Following ground breaking work on laser-based forward transfer (LIFT) of liquids by Serra and coworkers,[29–32] we have previously shown,[33] that by focusing a femtosecond (fs) NIR laser into a hydrogel underneath a layer of cells, a hydrogel jet is ejected from the gel. This process can be used to transfer small gel-droplets containing ≈10–30 cells to a target substrate with high cell viability.[33] Based on these findings, we have now elaborated a method, which allows the identification and selection of individual mammalian cells from a cell reservoir as well as the subsequent transfer of these cells to a target surface with single cell precision and a 93–99% cell-survival rate, depending on cell type and target substrate (see **Figure 1**a,b). We have integrated this setup into an inverted optical microscope (Figure 1a), which allows us to use cell morphology (e.g., cell shape or size) or fluorescence to select and sort individual cells from a heterogeneous cell population. For the cell transfer, we chose a laser wavelength of 1030 nm, which is at the center of the so-called biological optical window. At this wavelength, the interaction between photons and biological material reaches a minimum, and almost no laser energy is absorbed by cells or other biomaterials.[34,35] Yet, when a fs pulse of this wavelength is focused into an aqueous solution, the high photon density in the focus area leads to an optical breakdown, which eventually generates a rapidly expanding cavitation bubble.[36] The resulting hydrogel jet[30] can be used to transfer single or multiple cells from the hydrogel/cell reservoir to the target substrate.[33]

2. Results and Discussion

The example given in Figure 1c shows bright field microscopy images of B16F1 mouse melanoma cells on the surface of a hydrogel (histopaque 1083) reservoir before (left images) and after (middle) transferring the cells to the target surface. After the laser pulse has arrived, the single cell (top) or the group of five cells (bottom) have disappeared from the reservoir (middle row) and can be detected on the target surface (right). In both cases, a 600 fs laser pulse with 3 µJ pulse energy was focused ≈70 µm underneath the cell(s) to be transferred, as indicated by the red crosses (left images). With these parameters, hydrogel and cells within a radius of ≈25 µm around the lateral position of the laser focus were transferred to the target substrate. Consequently, if only one isolated cell is located within this ≈25 µm radius, a single cell is transferred to the target. If several cells are located within the ≈25 µm radius, all cells within this radius are transferred to the target. By choosing appropriate conditions for cell harvesting and reservoir preparation, for example, suitable trypsinization protocols and cell concentrations, a sufficient amount of isolated cells within the cell reservoir for single cell transfer is feasible (see Experimental Section for preparation details).

Previous approaches using LIFT technology to transfer and print mammalian cells,[37] either rely on inorganic sacrificial layers,[38–41] which are transferred together with the printed cells and which contaminate the target structure,[42] or they rely on UV lasers which frequently lead to DNA double strand breaks,[43] rendering these techniques potentially toxic or carcinogenic. While the irradiation of UV lasers has been screened to some extent by organic light absorbing layers, such as gelatin, reducing the number of cells showing DNA double strand breaks after transfer from 21.1% to 10.5%,[43] this amount of DNA double strand breaks in engineered tissue still poses a significant health risk for future in vivo applications. Our approach avoids these shortcomings by using fs NIR laser pulses in the biological optical window, which do not require inorganic sacrificial layers and do not induce DNA double strand breaks.[33] Only in the laser focus, the photon density is sufficient to initiate nonlinear absorption and an optical breakdown.[44] Outside of the focus, where no multiphoton absorption occurs, the 1030 nm laser pulses hardly interact with the cells. In addition, to our knowledge, none of the previously used approaches has achieved single cell precision.

To prove that we are indeed able to select and transfer single cells as well as to analyze the transfer process and further optimize the parameters of single cell and multi cell transfers, we used an upright rather than an inverted optical microscope configuration and integrated a second optical path perpendicular to the transfer path (Figure 1b). This second path allows for the time-resolved microscopic observation of the transfer process of individual, cell-laden hydrogel droplets. To obtain a sufficiently high temporal resolution, we used a delay generator, which triggered a frequency-doubled q-switched laser for time-delayed fluorescence illumination at a wavelength of 523 nm. Alternatively, a nanosecond spark flash-lamp for time-delayed white light illumination was triggered. This enabled the recording of side-view fluorescence or shadowgraphy images at defined delay times after arrival of the fs transfer pulse in a pump-and-probe approach, rendering 5 ns time resolution for side-view fluorescence images and 28 ns time resolution for shadowgraphy images (see Figure 1b and Experimental Section for details).

Figure 2a displays three fluorescence imaging time series of the transfer process recorded at 5 ns time resolution. The top row highlights an Alexa Flour 532-labeled B16F1 cell, 1, 3, 5, 7, 10, 15, and 20 µs after the arrival of the NIR transfer pulse. The middle row shows the transfer of a B16F1 cell, which is not fluorescently labeled. The bottom row shows the plain hydrogel jet without the presence of any cells. Both images on the right are close-ups of the images at 3 and 10 µs. To visualize the hydrogel jet in the fluorescence images, Alexa 532 was added to the hydrogel, obtaining a final concentration of 0.02 mM for all three time series (see Experimental Section for details of the cell and hydrogel staining). Here, the pulse energy of the fs transfer laser was set to 2 µJ and the focus depth to 52 µm. In the top row, the labeled cell can be clearly identified by the bright circular fluorescence signal at the tip of the hydrogel jet. The cell's fluorescence intensity at 10 µs corresponds to ≈4900 counts, using a 14-bit CCD camera, with a full well capacity of 16 000 e^-

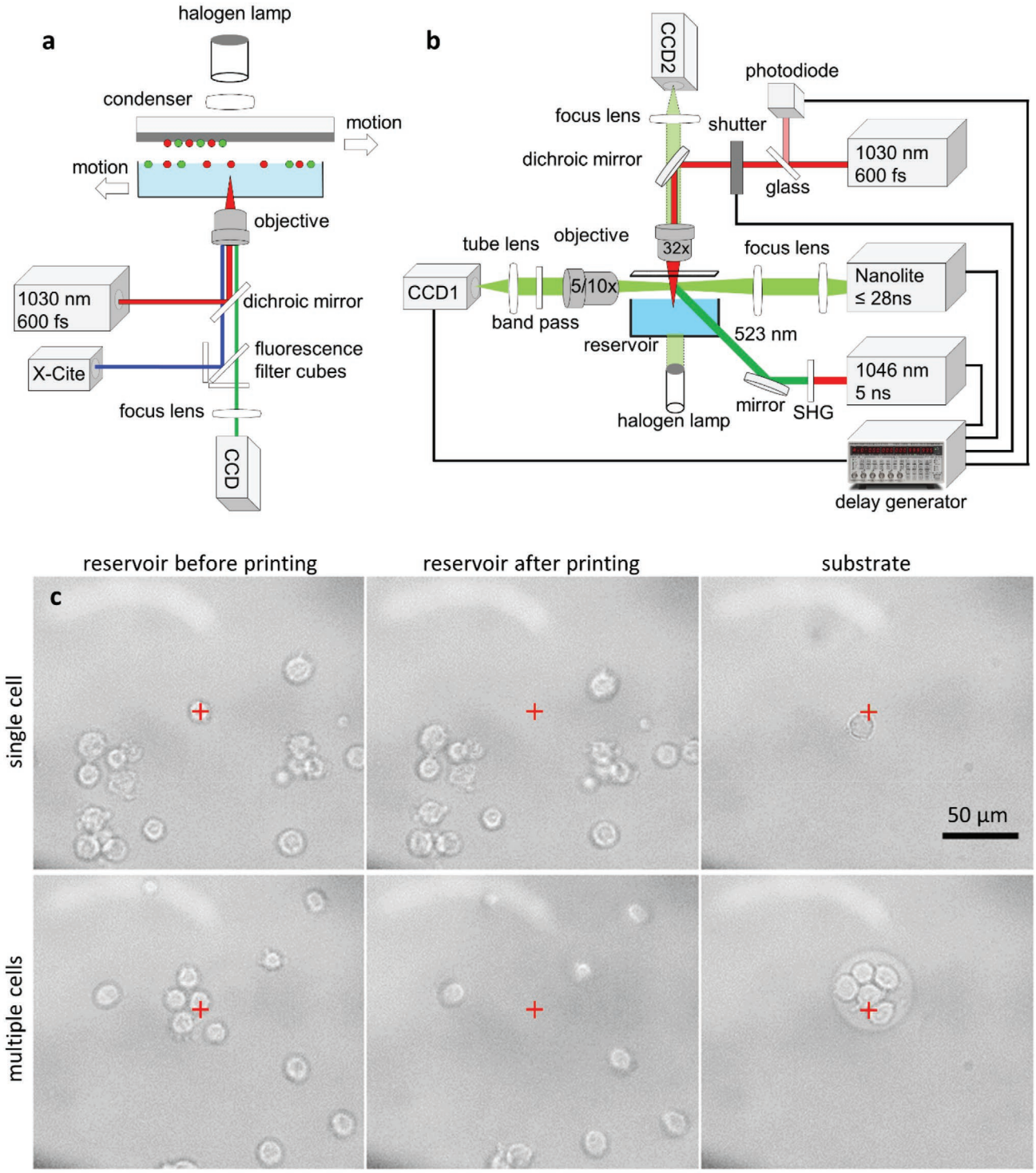

Figure 1. Laser-based transfer of single cells and of cell clusters. a) Laser-based cell-transfer setup combined with inverted optical microscopy for cell selection. b) Upright optical configuration, as used for time-resolved analysis of the transfer process shown in Figures 2a,c and 3e, and in Figures S1, S2, and S7, Supporting Information. c) Single (upper panel) and multiple (lower panel) B16F1 cells are identified with an optical microscope (bright field, 32× objective, NA = 0.6), selected and transferred from a hydrogel reservoir to a target substrate. Red crosses mark the center of the bright field images, which correspond to the laser focus position in the reservoir (left images). The laser pulse energy is 3 µJ and the focus depth is 70 µm. Scale bar for all micrographs = 50 µm.

and a gain of one. In the time series with the unstained cells (middle row), a black circle at the tip of the jet (≈900 counts @ 10 µs) indicates a lack of fluorescent molecules at the position where the (unstained) cell is located. If no cell is present (bottom row), only the fluorescence signal from the hydrogel (≈1500 counts @ 10 µs) can be observed. The horizontal stripes,

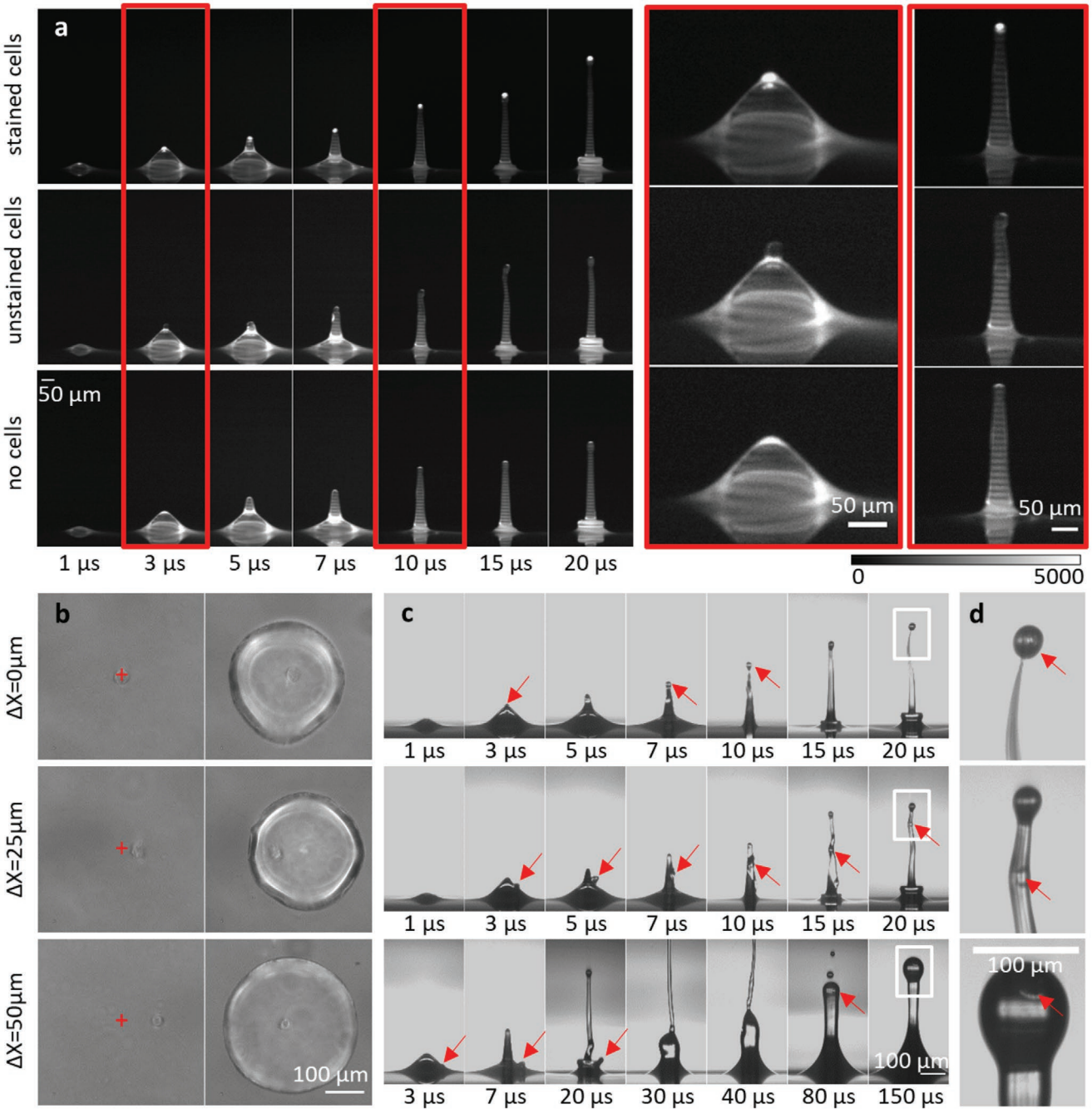

Figure 2. a) Time-resolved fluorescence images of the transfer of individual Alexa 532-labeled B16F1 cells (top row), unstained B16F1 cells (middle row), and pure hydrogel (bottom row). In all cases, Alexa 532 was added to the hydrogel, in order to visualize the hydrogel jet. Scale bars = 50 µm. (See also Figure S1, Supporting Information, for color-coded fluorescence intensities). b) Human tendon stem/progenitor cells (hTSPC) with different lateral offsets, Δx, between the cell and the focus position of the transfer laser, before (left) and after transfer (right). c) Time-resolved images of the transfer process of single hTSPCs with different lateral offsets, Δx, between cell and transfer laser and d) close-up images of the jet tip. Red arrows point at the transferred cells. Scale bars = 100 µm. Laser parameters (a–d): pulse energy = 2 µJ, focus depth = 52 µm.

which are present in all images, are most likely interference patterns caused by the ns illumination laser. Note that each time point shown corresponds to a new cell transfer, recorded with another delay time between NIR fs transfer pulse and a 5 ns pulse of the green illumination laser in the observation path. The fact that almost no jitter is observed within the three time series, demonstrates the high reproducibility and robustness of our transfer process. The subtle differences in jet shape between labeled und unlabeled cells observed at 3 µs (see close-up in Figure 2a) could be caused, for example, by slight differences in the initial z-position of the cells. Although the transfer of a cell from the reservoir to the target substrate requires

less than 100 µs per cell, manually searching for a cell takes ≈5 s, setting the laser focus another ≈5 s, and positioning of the acceptor surface takes further ≈10 s. Thus, the total time required per cell transfer is ≈20 s (mean ± SD of 69 transfers: 20.3 ± 6.5 s). Nevertheless, in a future setup, the whole process can be vastly accelerated by including an image recognition software, laser scanners, and fully automated positioning of the acceptor surface.

To explore the stability of the transfer process with respect to the focusing precision we switshed from murine to human primary cells and introduced a lateral offset, Δx, between the cell to be transferred and the focus position of the NIR fs transfer laser. Figure 2b shows three human tendon stem/progenitor cells (hTSPC) before and after the transfer process, with an offset Δx of 0, 25, and 50 µm between the x–y-position of the laser focus (indicated by a red cross) and the cell. In all three cases, the cell was successfully transferred to the target substrate using the same laser parameters as in Figure 2a. For a more detailed investigation of the transfer process with different offsets, we again used the optical inspection path perpendicular to the transfer direction, which is schematically depicted in Figure 1b. Instead of using the frequency-doubled q-switched ns laser, which we used for fluorescence illumination, we now used the white nanosecond spark flash-lamp for bright field illumination, rendering 28 ns time resolution. Figure 2c shows the time-resolved images of the transfer process for all three offsets. While for $\Delta x = 0$ µm the cell seems to be located at the very tip of the hydrogel jet, for $\Delta x = 25$ µm a small bump, indicated by red arrows, can be identified at the upper right side of the jet, which seems to correspond to the transferred cell. The close-up at 20 µs reveals a ≈15 µm circular object at ≈80% jet height (red arrow), which again seems to be the transferred cell. For $\Delta x = 50$ µm, a small bump, comparable to the one seen for 25 µm offset, can be observed at the lower right side of the hydrogel jet (again indicated by red arrows at 3–20 µs delay time). However, in this case, the cell is far away from the tip of the (thin) initial hydrogel jet and is not transferred with this first jet. Instead, the cell is now transferred to the target substrate with a much thicker second hydrogel jet, following the first jet ≈20 µs after the transfer pulse. The thin first hydrogel jet propagates at a velocity of 17.5 ± 0.5 m s^{-1} and reaches the target surface ≈60 µs after the transfer pulse, while the much thicker second jet propagates at an initial velocity of 5.2 ± 0.1 m s^{-1}, reaching the target surface ≈500 µs later (see Figure S2a,b, Supporting Information, for complete time series and a quantitative analysis of the transfer process). For $\Delta x = 0$ µm and $\Delta x = 25$ µm, the start of the second jet can be observed in the images recorded at 20 µs delay time. Note that because of the larger focus depth of ≈70 µm in the transfers shown in Figure 1c, the second jet did not reach the target surface, explaining why in this case only cells with up to 25 µm lateral offset from the focus position were transferred.

To investigate the printing precision, we used again human cells and printed rows of human mesenchymal stem cells (hMSCs) with predefined intercell distances of 50, 100, and 200 µm on a gelatin-coated substrate. As can be seen in **Figure 3**a, most cells deviate less than one cell diameter (≈14–32 µm for the hMSCS used here)[45–48] from their target positions, indicated by red crosses (cross size: 15 × 15 µm). A detailed analysis of the printing accuracy can be found in Figure S3, Supporting Information, and gives an overall positioning accuracy in our experiments of ±14.4 µm (root mean square deviation [RMSD] from the target position determined by 101 independent transfers), and a precision (standard deviation) of ±11.8 µm (see also Statistical Methods in the Experimental Section).

To investigate the cell viability of human primary cells after the transfer and as an example of using single cell printing to study cell–cell interactions, we printed hTSPCs on a collagen-coated substrate and carried out time-lapse video microscopy for 66 h after printing. Figure S4, Supporting Information, shows three rows of hTSPCs printed with intercell spacing of 50, 100, and 200 µm. After 5 and 10 h, the hTSPCs with 50 and 100 µm intercell spacing started to polarize and elongate toward neighboring cells, while the 200 µm separated cells remained isolated and were seemingly unaffected by their neighbors. This indicates paracrine and/or substrate mediated mechanical communication between the cells, stimulating cell elongation at intercell distances of 50 and 100 µm, while at larger intercell spacing, the biochemical and/or mechanical signals did not reach the neighboring cells. After 20 h and more, cells with an initial intercell spacing of 100 and 200 µm started migrating away from each other, while the 50 µm-spaced cells still remained in close proximity to each other and partially maintained physical cell–cell contacts (see also Figure S4 and Videos S1–S3, Supporting Information), only to disengage at later time points. This is most likely due to the lack of external guidance by the ECM. The cell–cell contacts observed for the 50 µm intercell distance, are crucial for structural organization and integrity of tendon tissue. In native tendon, the tenocytes, which in vivo derive from TSPCs, align themselves in parallel longitudinal rows separated by collagen fibers.[49] The cell–cell contact is mediated via gap and adherens junctions, which are associated to actin stress fibers. The orientation of those fibers aligns with the longitudinal cell orientation and thereby, specific mechano-sensitive signal transductions pathways are triggered allowing cells to sense the tensile loads in the tissue.[50–52] To engineer tendon tissue, the establishment of such cell–cell contacts is therefore critical to obtain functional tissue mimetic constructs.[53]

It should be pointed out, that even 66 h after the cell transfer, all hTSPCs were still migrating, indicating a cell-survival rate of 100% in this experiment. Additional live–dead assays based on propidium iodide staining of transferred cells (see Experimental Section and Figure S5, Supporting Information), as well as many more time-lapse experiments (data not shown) confirmed that an overall cell-survival rate of 92.7 ± 0.9% (mean and standard error of 65 cell transfers and 7 independent experiments) can be obtained for hTSPCs transferred to a collagen-coated substrate. For human papillary thyroid carcinoma cells (TPC1) transferred to a gelatin-coated substrate, we obtained a survival rate of 98.5 ± 0.4% (165 cells, 15 independent experiments). For B16F1 cells, which were transferred to a Matrigel-coated substrate in the upright optical configuration (Figure 1b), we obtained an effective survival rate of 96.5 ± 0.7% (134 cells, 13 independent experiments). This is consistent with literature values of other laser-based cell-transfer technologies.[54–56] However, unlike these other technologies, our approach cannot only

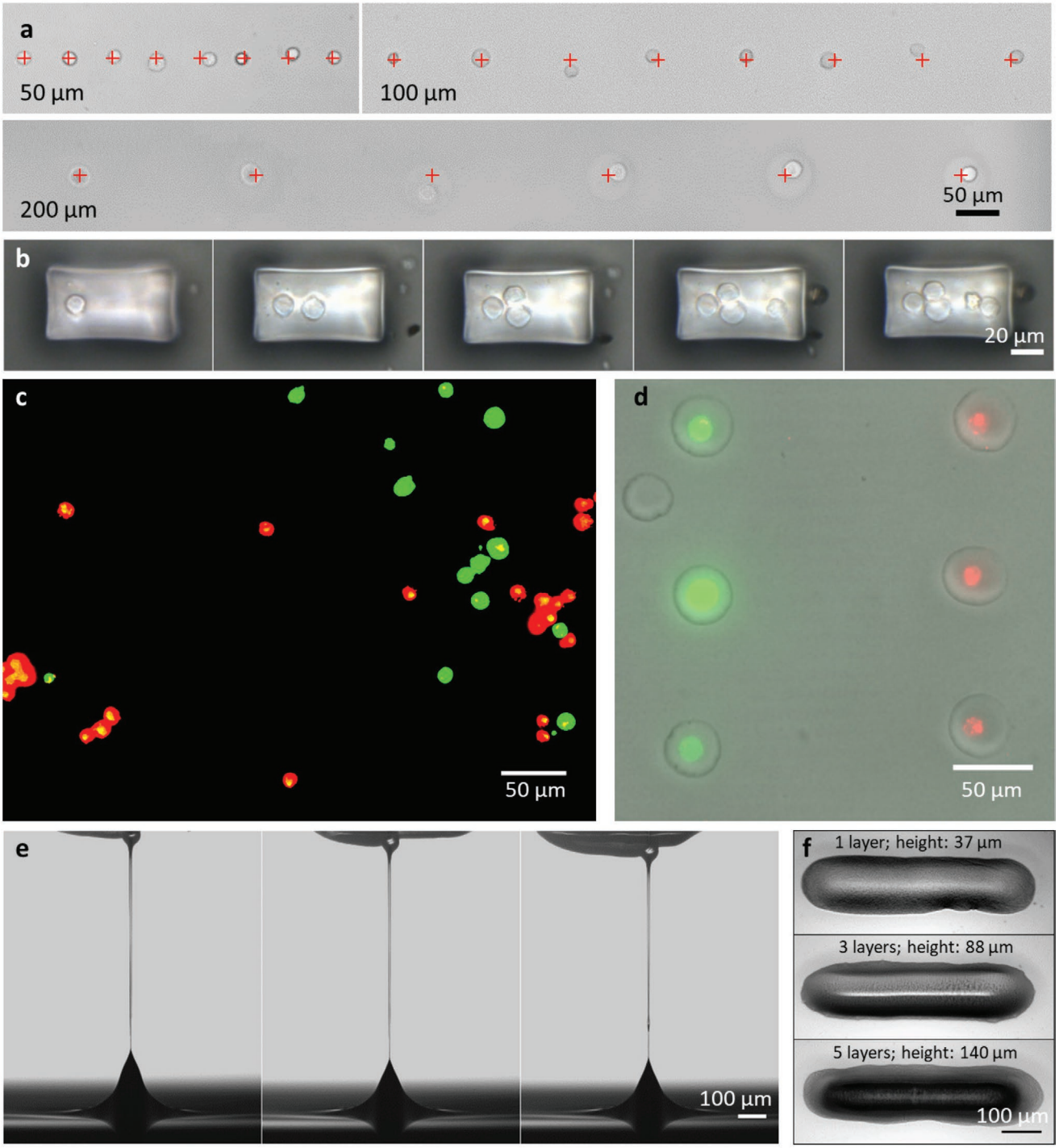

Figure 3. a) Precise positioning of cells (hMSCs) in rows with defined cell–cell distances. b) hMSCs placed one at a time on a prefabricated micro scaffold. c) Selection of GFP-labeled hMSCs and orange-labeled human TPC1 cells from a cell mixture and d) sorting them based on their fluorescent label. e–f) 3D printing of up to five layers of Pluronic F-127 (see also Video S4, Supporting information).

be used to select and transfer individual cells, but it also does not rely on inorganic light adsorbing material or UV radiation, which can contaminate the target structure[42] or induce double strand breaks in the cell's DNA.[43] Details of the propidium iodide staining used in the live–dead assays, as well as negative and positive controls can be found in the Analysis of Cell Viability and Statistical Methods subsections and in Figure S5, Supporting Information.

For the fabrication of functional tissue constructs, it is often necessary to precisely position mammalian cells within pre-manufactured scaffolds or guiding rails. This is highlighted in Figure 3b, where individual hMSCs were placed one by one in

a premanufactured cross-linked bovine serum albumin (BSA) scaffold.[57,58] Note that after the third cell was transferred to the BSA scaffold and placed in close proximity to the first and the second transferred cell, the second cell was slightly shifted. This was most likely driven by a hydrodynamic flow on the scaffold's surface, caused by the hydrogel carrying the third cell. Here, the test scaffold was premanufactured by two-photon stereolithography. In future setups, one might even envision using the NIR fs laser for both the cell transfer and two-photon stereolithography within the same setup or integrating an additional laser for two-photon stereolithography into the inverted microscope setup.

In addition to precisely position individual cells, our technique allows for the selection of individual cells prior to the transfer process based on size, morphology, or fluorescence signals. Figure 3c,d shows an example where GFP-labeled hMSCs and orange-labeled human papillary TPC1 were selected from a heterogeneous cell population (Figure 3c) and sorted on the target substrate based on their fluorescence. Other examples, showing cells sorted by size or where genetically modified cells were selected based on the intensity of a fluorescence marker, which is co-expressed with the gene of interest, are shown in Figure S6, Supporting Information.

To demonstrate, that our setup can not only be used to select, place, and print individual cells and hydrogels in 2D, but also to extend the printing process into 3D, we printed five layers of the biocompatible thermo-reversible hydrogel Pluronic F-127 on the target substrate (Figure 3e and Video S4, Supporting Information). Here, the hydrogel Pluronic F-127 was diluted to 15 wt% and cooled to 4 °C. At this temperature, the Pluronic solution has a viscosity of ≈40 mPas.[59] Upon arrival at the acceptor substrate, which was kept at room temperature (22 °C), the temperature of the Pluronic hydrogel increased to room temperature, driving the Pluronic hydrogel through its gel–sol transition and to a final viscosity, which is sufficient for stable 3D constructs. As can be seen in Figure 3f, the result is a well-defined 600 µm long, 120 µm wide line, which increases in height with every accumulated layer. To investigate whether our approach can also be used for the 3D printing of more viscous hydrogels, we investigated how the transfer kinetics are affected by the viscosity of the gels. Figure S7a, Supporting Information, shows the kinetics of the hydrogel jet for pure histopaque and for three different alginate concentrations (0.5%, 1% and 1.5% alginate dissolved in histopaque) with viscosities of 13, 48, 140, and 450 mPas, respectively, using 2, 3, and 4.2 µJ pulse energy. As expected, for 2 µJ pulse energy, the final jet velocity decreased from 18.8 ± 0.6 m s^{-1} for pure histopaque to 14 ± 0.6 m s^{-1} for 0.5% alginate and to 4.1 ± 0.3 m s^{-1} for the 1% alginate hydrogel (see Figure S7b, Supporting Information). For 1.5% alginate and 2 µJ pulse energy, the kinetic energy of the hydrogel jet is not sufficient to overcome the surface tension of the air–hydrogel interface and the jet collapses without leaving the hydrogel reservoir. Also a pulse energy of 3 µJ is still not sufficient for a successful transfer. However, if the laser pulse energy is increased to 4.2 µJ, even at 1.5% alginate concentration and a viscosity of 450 mPas, the jet overcomes the surface tension of the air–hydrogel interface, escaping from the hydrogel reservoir with a velocity of 4.9 ± 0.4 m s^{-1} (see Figure S7c, Supporting Information). Alginate is a frequently used hydrogel for bioprinting applications, where it is usually cross-linked with calcium, immediately after printing. At 1.5%, the alginate concentration is just high enough for 3D printing, if the alginate is cross-linked with calcium, for example, through a calcium containing hydrogel on the acceptor side.[60]

3. Conclusion

In summary, we have presented a new bioprinting method, which allows to select individual mammalian cells from a heterogeneous cell population and to position them with single cell precision and 93–99% cell-survival rates on a target substrate or a premanufactured scaffold. Our approach can readily be extended from 2D into 3D. At present, selecting the cell, focusing, and positioning of the target surface are the rate limiting steps. The integration into an inverted optical microscope setup, will allow for the use of automated image analysis and a cell recognition software in the future, which is a prerequisite for a fully automated process. The cell-transfer process alone requires less than 100 µs per cell, which would allow transfer rates of ≈10 kHz, and by using a multiplexing approach with fast laser scanners, one can envision even faster cell-transfer rates in the future, which are limited only by the repetition rate of the laser. This approach will thus enable the precise, fast, and cell-friendly fabrication of cell-chips, organs-on-a-chips, 3D organoids, and ultimately of functional tissue substitutes.

4. Experimental Section

Inverted Laser-Based Cell-Transfer Setup: For fs laser-induced single cell sorting and transfer, the fs laser beam (λ = 1030 nm, 600 fs, Spectra Physics, Rankweil, Austria) was coupled in an inverted epifluorescence microscope (Nikon Ti-E) by using a dichroic mirror (Figure 1a), which is highly reflective in the NIR but transmits visible light. The laser beam was focused through a 25×/0.95 water immersion objective (Leica HC FLUOTAR L 25×/0.95 W VISIR, Leica, Wetzlar, Germany) and mounted in a motorized objective revolver for vertical positioning. A motorized microscope-stage was used to scan the suspended cells in the reservoir in x–y-direction. Both, the reservoir and the acceptor surface were kept at 37 °C and 90% humidity inside a closed incubation chamber (Ibidi, Martinsried, Germany) to ensure cell viability and sterile conditions during the bioprinting process. Cell shape and size were recorded using bright field illumination. Additionally, a fluorescent light source (X-Cite 120 Q, EXFO La Forêt, France) was installed to monitor fluorescent-labeled cells and hydrogels. For image acquisition, a CCD camera (MMI CellCamera 1.4, MMI Eching, Germany) was used.

Upright Setup for Time-Resolved Analysis of the Laser-Based Cell Transfer: For time-resolved shadowgraphy and fluorescence imaging according to the pump-probe principle, the NIR fs pump-pulse was focused by a 32×/0.6 microscope objective (Leica Wetzlar, Germany). For shadowgraphy, the transfer process was probed in transmission with a pulsed 28 ns spark flash-lamp (Nanolite KL-L, High-Speed Photo-Systeme, Wedel, Germany). For fluorescence excitation, a collimated frequency-doubled q-switched laser pulse (wavelength 523 nm, pulse duration 5 ns, 40 µJ pulse energy, Mosquitoo, InnoLas Photonics, Germany) was used. The probe imaging system comprised of a microscope objective (M Plan Apo 5×/0.14 and 10×/0.28, Mitutoyo, Japan) perpendicular to the 523 nm excitation ns laser beam, an emission bandpass filter (555/20 ET Bandpass, Chroma, Bellows Falls, VT), a tube lens (TTL200-A, Thorlabs, Bergkirchen, Germany), and a 1.4 MP, 14-bit monochrome CCD camera (CCD1 in Figure 1b) with a full

well capacity of 16 000 and 6 e^- rms read out noise (PCO, Pixefly USB, Kelheim, Germany). Synchronization was accomplished by a photodiode (DET10A/M, Thorlabs) and a delay generator (DG645, Stanford Research Systems, Sunnyvale, CA). By illuminating the transparent reservoir from below with a halogen lamp, a bright field image of the cell distribution at the hydrogel surface was obtained with the confocal camera CCD2 (DMK 41BU02.H, Imaging Source, Bremen, Germany, see also Figure 1b). By moving the reservoir in x–y-direction the desired cells were selected. A separate x–y–z stage allowed for precise positioning of the transferred cell-laden droplets onto the acceptor slide. The distance between the hydrogel/cell surface and the acceptor slide amounted to 1 mm. The focus depth of the fs-laser pulse in the liquid was controlled by a motorized objective on a z-stage (LS-65, Physik Instrumente, Karlsruhe, Germany).

Cell Culture: hMSCs (SCP1 cell line),[61] murine skin melanoma cells (B16F1 cell line, ATCC, Wesel, Germany), human papillary thyroid carcinoma cells (TPC1cell line, ATCC, Wesel, Germany), and murine fibroblasts (NHI/3T3 cell line, ATCC, Wesel, Germany) were maintained in Dulbecco's modified eagle medium (DMEM, Biochrom, Germany) supplemented with 10% fetal bovine serum (FBS, Biochrom, Germany), 1% GlutaMAX (Thermo Fisher Scientific, Germering, Germany), and 1% Penicillin/Streptomycin (P/S, Biochrom, Berlin, Germany). hTSPCs were previously isolated from Achilles tendon and characterized in detail by Kohler et al.[62] The isolation of the cells was approved by the Ethical Commission of the LMU Medical Faculty (grant No. 166-08), and informed consent was obtained from the donors. hTSPCs were maintained in DMEM/HAMs F-12 medium (Biochrom, Germany) supplemented with 10% FBS, 1% GlutaMAX, 1% P/S, and 1% non-essential amino acids (Gibco, Germany). In routine cell culture, all cells were grown up to 80% confluency and maintained at 37 °C in 5% humidified CO_2. For passaging, cells were detached with 0.25% trypsin/0.02% EDTA solution (Biochrom, Germany).

Preparation of the Hydrogel Reservoir: To transfer living cells using the inverted optical configuration, 2×10^4 freshly detached cells were pelleted by centrifugation and suspended in 400 µL histopaque 1803 (Sigma-Aldrich, Deisenhofen, Germany). To detach cells, 0.25% trypsin/0.02% EDTA was used and the detachment was performed under microscopic control to ensure a complete detachment of the adherent cells, until only single cells remained in suspension. Detachment times were variable depending on the cell type. This suspension was transferred to a µ-Dish (µ-Dish 35 mm low, Ibidi, Martinsried, Germany), which served as reservoir for cell transfer. Due to their lower mass-density, the cells concentrated at the surface of the histopaque 1803. For jet visualization with shadowgraphy, a rectangular, transparent dish (DIC Lid, Ibidi, Martinsried, Germany) was used as reservoir, which was filled with cell-laden hydrogel (1×10^4 cells/mL in histopaque 1083). For fluorescence-based jet visualization, 5 mL histopaque 1083 were mixed with 10 µL fluorescent dye (Alexa) 532-I amine-reactive succinimidyl ester (Abnova, Germany, 10 mM dissolved in DMSO, maximum excitation/emission wavelength of 542/558 nm), yielding a final concentration of 0.02 mM. For cell staining, 10^5 B1F1 cells were pelleted by centrifugation. The cell pellet was suspended in 10 µL of the same fluorescent dye and incubated under gentle agitation for 2 h at 37 °C. The stained cells were added to the stained hydrogel within the reservoir. For printing of high viscous hydrogel, histopaque 1083 was supplemented with alginic acid sodium salt from brown algae (Sigma-Aldrich) in concentrations up to 1.5%.

Viscosity Measurement: The viscosity measurement of alginate hydrogels was carried out at room temperature (21 °C) using the rotational viscometer RC01/02 (Rheotec, Dresden, Germany) at a rotational speed of 200 rpm. For the measurement of 1.5% alginate hydrogel samples, the viscometer was equipped with the L4 standard spindle, while for the 1% alginate hydrogel the spindle was changed to the L3 standard spindle, and both, the 0.5% hydrogel and the pure histopaque 1083 as control, were measured using the L2 standard spindle.

Preparation of the Acceptor Surface: For jet visualization according to the pump-probe principle, a standard coverslip with a thickness of 170 µm was used as acceptor slide. To print living cells, a hydrogel-coated coverslip or a Petri dish (TC Dish 60, Standard Sarstedt, Germany) served as an acceptor surface to protect the transferred cells from drying out. The respective hydrogel depended on the printed cell type. When printing TPC1 cells, gelatin (Sigma-Aldrich, Germany) was used for coating. The gelatin was dissolved in PBS (10% w/v) at ≈50 °C, homogenously dispersed on the acceptor surface and then cooled to 4 °C for 15 min, to form a film of ≈100 µm thickness. The acceptor surface for hTSPCs was coated with 0.5% collagen (Collagen G1, MATRIX BioScience, Germany). The collagen stock solution was gently mixed with neutralizing buffer (1 mL of 0.7 M sodium hydroxide solution, 1 mL of 1 M HEPES buffer, and 2 mL 10× DMEM, pH adjusted to 7.9–8.05) at a ratio of 4:1. 5 mL of this mixture were homogenously dispersed on the bottom of the Petri dish and then incubated over night at 37 °C. To print B16F1 cells, Matrigel (BD Biosciences, Heidelberg, Germany) was used as an acceptor coating. Matrigel was thawed at 4 °C overnight, 100 µL was evenly dispersed in the precooled Petri dish and then incubated at 37 °C for 10 min to obtain a ≈100 µm hydrogel layer.

Analysis of Cell Viability: The survival rate of the transferred cells was evaluated as described in Zhang et al.[33] and is briefly summarized below: To detect dead cells, the hydrogel on the acceptor slide was supplemented with two droplets of propidium iodide ReadyProbes reagent (PI R37108, Thermo Fischer, Germering, Germany), per mL hydrogel solution. Intact cells rejected PI; in dead cells PI bound to DNA and caused a red fluorescence. After cell transfer, the acceptor surface was incubated at 37 °C for 15 min to allow PI staining. Dead cells were visualized by fluorescence microscopy using an inverted optical microscope (Nikon Ti-E). The viability of non-transferred cells remaining in the reservoir was also investigated by PI staining. Live and dead cells were counted using a standard hemocytometer chamber (Brand, Wertheim, Germany) in the fluorescence microscope. For hTSPC and TPC1 cells, (additional) PI staining of all cells in the cell reservoir prior to the laser transfer served as negative control and ensured that only viable cells were transferred in the cell viability experiments. For B16F1 cells, the viability was determined using the upright bioprinting configuration, which did not allow selecting 100% viable cells prior to transfer. Here, the numbers of live and dead cells after the transfer were determined in the inverted fluorescence microscope, as described above. The effective cell-survival rate was then determined by dividing the percentage of viable cells after transfer (92.1%) by the percentage of viable cells without laser transfer (95.2%), which was determined in an independent negative control experiment using PI staining of non-transferred cells. To ensure the effectiveness of PI staining, cells were deliberately killed during transfer, by setting the laser focus to only 35 µm and then stained with PI in a positive control experiment (see Figure S5, Supporting Information, for PI staining of transferred cells, as well as negative and positive control experiments).

To determine the cell-survival rate via time-lapse microscopy, the hydrogel-coated acceptor slide containing the transferred cells was placed in an incubation chamber, providing 37 °C and 5% humidified CO_2 atmosphere (Pecon, Erbach, Germany). This chamber was mounted on an inverted optical microscope (Observer Z.1, Carl Zeiss, Göttingen, Germany) and a first image was recorded. After 15 min, 3 mL of DMEM cell culture medium for B16F1 cells and DMEM/HAMs F-12 medium for hTSPCs were gently added. From now on, microscopy images were collected in 20 min intervals for up to 66 h. The images were taken using an Orca Flash 4.0 scientific CMOS camera (Hamamatsu, Herrsching, Germany). In time-lapse images, activities such as active cell spreading, polarization, migration, and proliferation were used as indicator of cell viability.

Cell Staining: For phalloidin and DAPI stainings, the cells on the acceptor surface after 66 h were washed with PBS containing Ca^{2+}/Mg^{2+} (Biochrom, Germany), fixed with 3.7% formaldehyde (Carl Roth, Germany) for 15 min at RT and then washed thrice with PBS. For permeabilization, cells were incubated with 0.5% Triton-X 100 (Sigma Aldrich) in PBS for 10 min at RT. The cells were submersed in the staining solution containing Atto594-Phalloidin (Atto-Tec GmbH, Germany) in a final concentration of 200 ng mL^{-1} and DAPI (AppliChem GmbH, Germany) in a final concentration of 10 ng mL^{-1} in PBS, incubated for

20 min at RT, washed thrice with PBS, air-dried, and mounted with ProLong Diamond Antifade Mountant (Thermo Fisher Scientific, Germany). To visualize F-actin in living cells, NIH/3T3 fibroblasts were transfected with the plasmid (pCMV-LifeAct-TagRFP, Ibidi, Germany) using the Torpedo^{DNA} transfection reagent (Ibidi, Germany). Sorting of the LifeAct expressing cells from non-expressing cells was done 48 h after transfection. For orange labeling of TPC1 cells, the Cell Explorer Live Cell Tracking Kit Orange (AAT Bioquest, Sunnyvale, USA) was used according to the manufacturer's instructions.

Preparation of the Pluronic F-127 for Printing of Three-Dimensional Structures: Dissolved Pluronic hydrogel is well-suited for 3D printing due to its thermo-responsive properties and fast gelation time, which can be adjusted by temperature and concentration.[59] For 3D printing with the authors' setup, Pluronic F-127 (Sigma Aldrich, Deisenhofen, Germany) was dissolved in PBS to a final concentration of 15 wt% and stored at 4 °C overnight. At this temperature, the hydrogel stayed liquid in the reservoir. The upright setup (see Figure 1b) was used to print 3D structures with Pluronic. Upon transfer to the acceptor slide, the Pluronic hydrogel underwent a fast gelation as the transferred droplets reached room temperature very quickly.

Preparation of Protein-Based Three-Dimensional Micro Scaffolds for Targeted Seeding of Single Cells: 3D micro scaffolds with a length of 80 µm, a width of 40 µm, and a height of 100 µm were printed with BSA-based resin and rose bengal as photo-initiator using the Nanoscribe GT two-photon stereolithography device (Nanoscribe, Karlsruhe, Germany). BSA resin preparation and high-resolution 3D printing were conducted as described elsewhere.[57] In brief, 40 wt% BSA stock solution was mixed with 85 mM rose bengal stock solution in the ratio 9:1. A droplet of this suspension was placed on a 170 µm thick glass slide. The 3D scaffolds were then printed using the dip-in mode. After completing the printing process, subsequent resin was washed away and scaffolds were stored in PBS at 4 °C until further usage.

Statistical Methods: Cell-survival rates were obtained by dividing the number of viable cells after cell transfer by the total number of cells transferred for each cell and substrate type. Cell viability was quantified with the propidium iodide ReadyProbes reagent life–dead assays (PI R37108, Thermo Fischer, Germering, Germany), as described above. As mentioned above, for hTSPC and TPC1 cells, additional PI staining of all cells in the cell reservoir prior to the laser transfer ensured that 100% viable cells were transferred for cell viability analysis. For B16F1 cells, the survival rate was determined in the upright configuration, which did not allow selecting 100% viable cells prior to transfer. Here, the effective cell-survival rate was therefore determined by dividing the percentage of viable cells after transfer (92.1%) by the percentage of viable cells without laser transfer (95.2%), which was determined in an independent negative control experiment using PI staining of non-transferred cells (see also Analysis of Cell Viability).

Printing accuracy was determined as the root mean square deviation (RMSD) from the target position:

$$\mathrm{RMSD} = \sqrt{\frac{1}{n}\sum_{i=1}^{n}\left[(x_i - x_0)^2 + (y_i - y_0)^2\right]} \quad (1)$$

where (x_i, y_i) were the individual cell positions, and (x_0, y_{i0}) designated the target position.

Printing precision was determined as the RMSD from mean cell position, corresponding to the standard deviation (SD) of printed cells:

$$\mathrm{SD} = \sqrt{\frac{1}{n}\sum_{i=1}^{n}\left[\left(x_i - \bar{x}\right)^2 + \left(y_i - \bar{y}\right)^2\right]} \quad (2)$$

where (x_i, y_i) were individual cell positions, and $(\bar{x}, \bar{y})$ designated the mean cell position.

Aspect ratio of cells of Figure S4, Supporting Information, was determined as the ratio between of length divided by width of individual single cells.

Supporting Information

Supporting Information is available from the Wiley Online Library or from the author.

Acknowledgements

The authors thank Conny Hasselberg-Christoph for technical assistance, Petra Schwille for support and access to the microfabrication facilities at the Max-Planck-Institute of Biochemistry, and Thomas Hellerer and Stefan Niehren for helpful discussions and support. J.Z. would like to acknowledge the coworkers of the Lasercenter at Munich University of Applied Sciences for valuable discussion on laser technology. The authors acknowledge financial support through the research focus "Herstellung und biophysikalische Charakterisierung dreidimensionaler Gewebe – CANTER" of the Bavarian State Ministry for Science and Education. J.Z. and A.E. acknowledge financial support by the Bavarian Academic Forum (BayWISS) – Doctoral Consortium "Gesundheit" and "Ressourceneffizienz und Werkstoffe", both funded by the Bavarian State Ministry of Science and the Arts. D.D. acknowledges the support of the EU H2020-WIDESPREAD-05-2017-Twinning Grant "Achilles: Overcoming specific weakness in tendon biology to design advanced regenerative therapies" Proposal No. 810850 as well as the H2020-NMBP-22-2018 Proposal No. 814444 MEFISTO.

Open access funding enabled and organized by Projekt DEAL.

Conflict of Interest

The authors declare no conflict of interest.

Data Availability Statement

Data available on request from the authors.

Keywords

single cell printing, single cell sorting, 3D bioprinting, three-dimensional printing, tissue engineering

Received: February 16, 2021
Published online: March 26, 2021

[1] L. Ionov, *Adv. Healthcare Mater.* **2018**, *7*, 1800412.
[2] C. Onofrillo, S. Duchi, C. D. O'Connell, R. Blanchard, A. J. O'Connor, M. Scott, G. G. Wallace, P. F. M. Choong, C. D. Bella, *Biofabrication* **2018**, *10*, 045006.
[3] L. Moroni, J. A. Burdick, C. Highley, S. J. Lee, Y. Morimoto, S. Takeuchi, J. J. Yoo, *Nat. Rev. Mater.* **2018**, *3*, 21.
[4] T. Liu, R. Yao, Y. Pang, W. Sun, *J. Tissue Eng. Regener. Med.* **2019**, *13*, 2101.
[5] K. Jakab, F. Marga, R. Kaesser, T. H. Chuang, H. Varadaraju, D. Cassingham, S. Lee, A. Forgacs, G. Forgacs, *Mater. Today Sustainability* **2019**, *5*, 100018.
[6] W. Sun, B. Starly, A. C. Daly, J. A. Burdick, J. Groll, G. Skeldon, W. Shu, Y. Sakai, M. Shinohara, M. Nishikawa, J. Jang, D. W. Cho, M. Nie, S. Takeuchi, S. Ostrovidov, A. Khademhosseini, R. D. Kamm, V. Mironov, L. Moroni, I. T. Ozbolat, *Biofabrication* **2020**, *12*, 022002.
[7] L. Papadimitriou, P. Manganas, A. Ranella, E. Stratakis, *Mater. Today Bio* **2020**, *6*, 100043.

[8] P. L. Graney, S. Ben-Shaul, S. Landau, A. Bajpai, B. Singh, J. Eager, A. Cohen, S. Levenberg, K. L. Spiller, *Sci. Adv.* **2020**, *6*, eaay6391.
[9] D. E. Discher, D. J. Mooney, P. W. Zandstra, *Science* **2009**, *324*, 1673.
[10] T. Graf, T. Enver, *Nature* **2009**, *462*, 587.
[11] E. H. Barriga, K. Franze, G. Charras, R. Mayor, *Nature* **2018**, *554*, 523.
[12] P. Friedl, S. Alexander, *Cell* **2011**, *147*, 992.
[13] R. Reuten, S. Zendehroud, M. Nicolau, L. Fleischhauer, A. Laitala, S. Kiderlen, D. Nikodemus, L. Wullkopf, S. R. Nielsen, S. McNeilly, C. Prein, M. Rafaeva, E. M. Schoof, B. Furtwängler, B. T. Porse, H. Kim, K. J. Won, S. Sudhop, K. W. Zornhagen, F. Suhr, E. Maniati, O. M. T. Pearce, M. Koch, L. B. Oddershede, T. V. Agtmael, C. D. Madsen, A. E. Mayorca-Guiliani, W. Bloch, R. R. Netz, H. Clausen-Schaumann, J. T. Erler, *Nat. Mater.* **2021**, https://doi.org/10.1038/s41563-020-00894-0.
[14] F. Lautenschläger, M. Piel, *Curr. Opin. Cell Biol.* **2013**, *25*, 116.
[15] J. A. Park, S. Yoon, J. Kwon, H. Now, Y. K. Kim, W. J. Kim, J. Y. Yoo, S. Jung, *Sci. Rep.* **2017**, *7*, 14610.
[16] J. Nie, Q. Gao, J. Fu, Y. He, *Adv. Healthcare Mater.* **2020**, *9*, 1901773.
[17] S. Mao, Y. Pang, T. Liu, Y. Shao, J. He, H. Yang, Y. Mao, W. Sun, *Biofabrication* **2020**, *12*, 042001.
[18] S. V. Murphy, A. Atala, *Nat. Biotechnol.* **2014**, *32*, 773.
[19] K. Zhang, C. K. Chou, X. Xia, M. C. Hung, L. Qin, *Proc. Natl. Acad. Sci.* **2014**, *111*, 2948.
[20] I. Leibacher, J. Schoendube, J. Dual, R. Zengerle, P. Koltay, *Biomicrofluidics* **2015**, *9*, 024109.
[21] A. Gross, J. Schöndube, S. Niekrawitz, W. Streule, L. Riegger, R. Zengerle, P. Koltay, *J. Lab. Autom.* **2013**, *18*, 504.
[22] A. Yusof, H. Keegan, C. D. Spillane, O. M. Sheils, C. M. Martin, J. J. O'Leary, R. Zengerle, P. Koltay, *Lab Chip* **2011**, *11*, 2447.
[23] Y. K. Kim, J. A. Park, W. H. Yoon, J. Kim, S. Jung, *Biomicrofluidics* **2016**, *10*, 064110.
[24] B. Kang, J. Shin, H.-J. Park, C. Rhyou, D. Kang, S.-J. Lee, Y.-s Yoon, S.-W. Cho, H. Lee, *Nat. Commun.* **2018**, *9*, 5402.
[25] P. Delsing, A. N. Cleland, M. J. A. Schuetz, J. Knörzer, G. Giedke, J. I. Cirac, K. Srinivasan, M. Wu, K. C. Balram, C. Baüerle, T. Meunier, C. J. B. Ford, P. V. Santos, E. Cerda-Méndez, H. Wang, H. J. Krenner, E. D. S. Nysten, M. Weiß, G. R. Nash, L. Thevenard, C. Gourdon, P. Rovillain, M. Marangolo, J. Y. Duquesne, G. Fischerauer, W. Ruile, A. Reiner, B. Paschke, D. Denysenko, D. Volkmer, A. Wixforth, H. Bruus, M. Wiklund, J. Reboud, J. M. Cooper, Y. Q. Fu, M. S. Brugger, F. Rehfeldt, C. Westerhausen, *J. Phys. D: Appl. Phys.* **2019**, *52*, 353001.
[26] S. M. Naseer, A. Manbachi, M. Samandari, P. Walch, Y. Gao, Y. S. Zhang, F. Davoudi, W. Wang, K. Abrinia, J. M. Cooper, A. Khademhosseini, S. R. Shin, *Biofabrication* **2017**, *9*, 015020.
[27] Z. Ma, A. W. Holle, K. Melde, T. Qiu, K. Poeppel, V. M. Kadiri, P. Fischer, *Adv. Mater.* **2020**, *32*, 1904181.
[28] X. Ding, J. Shi, S. C. S. Lin, S. Yazdi, B. Kiraly, T. J. Huang, *Lab Chip* **2012**, *12*, 2491.
[29] M. Duocastella, J. M. Fernández-Pradas, J. L. Morenza, D. Zafra, P. Serra, *Sens. Actuators, B* **2010**, *145*, 596.
[30] M. Duocastella, A. Patrascioiu, J. M. Fernández-Pradas, J. L. Morenza, P. Serra, *Opt. Express* **2010**, *18*, 21815.
[31] P. Serra, A. Piqué, *Adv. Mater. Technol.* **2019**, *4*, 1800099.
[32] J. M. Fernández-Pradas, C. Florian, F. Caballero-Lucas, P. Sopeña, J. L. Morenza, P. Serra, *Appl. Surf. Sci.* **2017**, *418*, 559.
[33] J. Zhang, B. Hartmann, J. Siegel, G. Marchi, H. Clausen-Schaumann, S. Sudhop, H. P. Huber, *PLoS One* **2018**, *13*, e0195479.
[34] F. A. Duck, *Physical Properties of Tissues: A Comprehensive Reference Book*, Institute of Physics and Engineering in Medicine, York, UK **2012**, pp. 57–61.
[35] R. W. Waynant, *Lasers in Medicine*, CRC Press, Boca Raton, FL, USA **2001**.
[36] A. Vogel, J. Noack, G. Hüttman, G. Paltauf, *Appl. Phys. B: Lasers Opt.* **2005**, *81*, 1015.
[37] A. A. Antoshin, S. N. Churbanov, N. V. Minaev, D. Zhang, Y. Zhang, A. I. Shpichka, P. S. Timashev, *Bioprinting* **2019**, *15*, e00052.
[38] L. Koch, O. Brandt, A. Deiwick, B. Chichkov, *Int. J. Bioprint.* **2017**, *3*, 42.
[39] L. Koch, A. Deiwick, S. Schlie, S. Michael, M. Gruene, V. Coger, D. Zychlinski, A. Schambach, K. Reimers, P. M. Vogt, B. Chichkov, *Biotechnol. Bioeng.* **2012**, *109*, 1855.
[40] L. Koch, A. Deiwick, B. Chichkov, *BioNanomaterials* **2014**, *15*, 71.
[41] V. Keriquel, H. Oliveira, M. Rémy, S. Ziane, S. Delmond, B. Rousseau, S. Rey, S. Catros, J. Amédée, F. Guillemot, J. C. Fricain, *Sci. Rep.* **2017**, *7*, 1778.
[42] P. Serra, J. M. Fernández-Pradas, M. Colina, M. Duocastella, J. Domínguez, J. L. Morenza, *J. Laser Micro/Nanoeng.* **2006**, *1*, 236.
[43] R. Xiong, Z. Zhang, W. Chai, D. B. Chrisey, Y. Huang, *Biofabrication* **2017**, *9*, 024103.
[44] A. Vogel, J. Noack, K. Nahen, D. Theisen, S. Busch, U. Parlitz, D. X. Hammer, G. D. Noojin, B. A. Rockwell, R. Birngruber, *Appl. Phys. B: Lasers Opt.* **1999**, *68*, 271.
[45] B. Alberts, A. Johnson, J. Lewis, M. Raff, K. Roberts, P. Walter, *Molecular Biology of the Cell*, 5th ed., Taylor & Francis, London **2007**.
[46] D. A. Guertin, D. M. Sabatini, *eLS* **2006**, 1, https://doi.org/10.1038/npg.els.0003359.
[47] Z. Yin, J. J. Hu, L. Yang, Z. F. Zheng, C. R. An, B. B. Wu, C. Zhang, W. L. Shen, H. H. Liu, J. L. Chen, B. C. Heng, G. J. Guo, X. Chen, H. W. Ouyang, *Sci. Adv.* **2016**, *2*, e1600874.
[48] J. Ge, L. Guo, S. Wang, Y. Zhang, T. Cai, R. C. H. Zhao, Y. Wu, *Stem Cell Rev. Rep.* **2014**, *10*, 295.
[49] D. Docheva, S. A. Müller, M. Majewski, C. H. Evans, *Adv. Drug Delivery Rev.* **2015**, *84*, 222.
[50] A. D. Waggett, M. Benjamin, J. R. Ralphs, *Eur. J. Cell Biol.* **2006**, *85*, 1145.
[51] C. M. McNeilly, A. J. Banes, M. Benjamin, J. R. Ralphs, *J. Anat.* **1996**, *189*, 593.
[52] J. R. Ralphs, A. D. Waggett, M. Benjamin, *Matrix Biol.* **2002**, *21*, 67.
[53] S. H. Richardson, T. Starborg, Y. Lu, S. M. Humphries, R. S. Meadows, K. E. Kadler, *Mol. Cell. Biol.* **2007**, *27*, 6218.
[54] J. A. Barron, B. R. Ringeisen, H. Kim, B. J. Spargo, D. B. Chrisey, *Thin Solid Films* **2004**, *453–454*, 383.
[55] L. Koch, S. Kuhn, H. Sorg, M. Gruene, S. Schlie, R. Gaebel, B. Polchow, K. Reimers, S. Stoelting, N. Ma, P. M. Vogt, G. Steinhoff, B. Chichkov, *Tissue Eng., Part C* **2010**, *16*, 847.
[56] B. R. Ringeisen, H. Kim, J. A. Barron, D. B. Krizman, D. B. Chrisey, S. Jackman, R. Y. C. Auyeung, B. J. Spargo, *Tissue Eng.* **2004**, *10*, 483.
[57] A. Erben, M. Hörning, B. Hartmann, T. Becke, S. A. Eisler, A. Southan, S. Cranz, O. Hayden, N. Kneidinger, M. Königshoff, M. Lindner, G. E. M. Tovar, G. Burgstaller, H. Clausen-Schaumann, S. Sudhop, M. Heymann, *Adv. Healthcare Mater.* **2020**, *9*, 2000918.
[58] S. Engelhardt, E. Hoch, K. Borchers, W. Meyer, H. Krüger, G. E. M. Tovar, A. Gillner, *Biofabrication* **2011**, *3*, 025003.
[59] E. Gioffredi, M. Boffito, S. Calzone, S. M. Giannitelli, A. Rainer, M. Trombetta, P. Mozetic, V. Chiono, *Proc. CIRP* **2016**, *49*, 125.
[60] H. Li, S. Liu, L. Li, *Int. J. Bioprint.* **2016**, *2*, 54.
[61] W. Böcker, F. Haasters, D. Docheva, M. Locher, Z. Yin, W. Mutschler, C. Popov, O. Rossmann, M. Wierer, I. Drosse, M. Schieker, *J. Cell. Mol. Med.* **2008**, *12*, 1347.
[62] J. Kohler, C. Popov, B. Klotz, P. Alberton, W. C. Prall, F. Haasters, S. Müller-Deubert, R. Ebert, L. Klein-Hitpass, F. Jakob, M. Schieker, D. Docheva, *Aging Cell* **2013**, *12*, 988.